

Sensitivity analysis of sea scallop larvae trajectories to hydrodynamic model configuration on Georges Bank and adjacent coastal regions

RUCHENG C. TIAN^{1,*}, CHANGSHENG CHEN^{1,2}, KEVIN D.E. STOKESBURY¹, BRIAN ROTHSCHILD¹, QICHUN XU¹, SONG HU¹, GEOFFREY COWLES¹, BRADLEY P. HARRIS¹ AND MICHAEL C. MARINO II¹

*¹Department of Fisheries Oceanography
School for Marine Science and Technology
University of Massachusetts Dartmouth
706 South Rodney French Blvd.
New Bedford, MA 02744, USA*

*²Marine Ecosystem and Environmental Laboratory
Shanghai Ocean University
999 Hucheng Huan Road
201306, Shanghai, China*

*Correspondence:

Rucheng Tian
Department of Fisheries Oceanography
School for Marine Science and Technology
706 South Rodney French Blvd.
New Bedford, MA 02744, USA.

rtian@umassd.edu

Phone: 1-508-910-6310

Fax: 1-508-910-6371

Running title: Scallop larvae dispersal modeling on Georges Bank

ABSTRACT

The previous larval-trajectory modeling studies on Georges Bank were assessed through process-oriented Lagrangian-tracking comparison experiments using the high-resolution Gulf of Maine/Georges Bank Finite-Volume Coastal Ocean Model (GOM-FVCOM). The results indicate that in a strong nonlinear system such as Georges Bank, the passive tracer movement is driven by a fully three-dimensional Lagrangian flow field that varies in space and time due to large tidal excursion and steep bottom topography. The particle tracking methods developed based on the assumption of weak nonlinearity of the flow field are not applicable to Georges Bank. The results of previous larval transport studies driven by circulation fields constructed under weak-nonlinearity assumption need to be interpreted with caution. In the present work, the influence of model physical setups on sea scallop larval dispersal and settlement on Georges Bank and adjacent shelf regions is examined. Distinct differences in the spatial distribution of the passive larvae predicted by the model under various physical conditions suggest that a fully nonlinear model driven by realistic spatially and temporally varying forcing should be employed for Lagrangian-based studies of fishery population dynamics on Georges Bank.

Key words: Individual-based model, Larval dispersion, Lagrangian tracking, Georges Bank.

INTRODUCTION

Individual-Based Models (IBM) are widely used to study the influence of fish larvae dispersion and retention on fish recruitment in coastal oceans. In an IBM, larvae are treated as individuals and tracked following the Lagrangian flow velocity predicted by a hydrodynamic ocean model. The reliability of larval transport and settlement prediction depends upon the robustness of the predicted Lagrangian flow field. In previous fish larvae and zooplankton modeling studies on Georges Bank (GB) (Fig. 1), the Lagrangian currents used to track individuals were assumed to be either the residual flow constructed by summing an Eulerian residual current and a first-order Stokes velocity (Miller et al., 1998) or the vector sum of a model-predicted barotropic semidiurnal M_2 tidal current and the climatologically-driven steady flow field (Werner et al., 1993; Tremblay et al., 1994). The first approach was valid for weak nonlinear circulation in which the Stokes velocity is one order of magnitude weaker than the Eulerian velocity. The second approach included the nonlinearity of the major tidal motion on GB, but ignored the influence of realistic temporal and spatial variation of surface forcing. Several questions were raised about these simplifications when we were developing a model to study the interannual variability of sea scallop (*Placopecten magellanicus*) larvae dispersal and settlement on GB. First, can the Lagrangian velocity developed under the theory of weak nonlinearity be applied to GB? Second, do the water currents driven by a bi-monthly averaged wind stress and a bi-monthly averaged hydrographic field realistically represent the Lagrangian flow field over GB? Third, when trajectories on the time scale of larval dispersal are concerned, should the influence of tidal forcing by other major semi-diurnal and diurnal tidal constituents be included?

The nature of the Lagrangian currents over GB has been intensively studied in the last decades. Loder et al. (1997) tracked neutrally buoyant particles using a three-dimensional (3D) flow field and found that the Stokes drift is the same order of magnitude as the Eulerian residual currents on GB, and thus the Lagrangian velocity should be calculated using a fully nonlinear approach. Chen and Beardsley (1998) found from their 2D model experiments that under stratified conditions, due to the interaction between the Eulerian and Stokes velocity over steeply-sloping bottom topography, the direction of the Lagrangian velocity on the northern flank of GB can be opposite to the local Eulerian velocity. This finding was supported by a 3D stratified experiment conducted by Chen et al. (2003a). These experiments demonstrate that the flow field on GB is characterized by strong nonlinearity so that particle tracking should be conducted by taking the spatial and temporal variation of tidal motion into account.

A modified meso-scale meteorological model (MM5) was applied to construct the high-resolution meteorological forcing at the surface. The model was implemented and validated for the GOM/GB region and predicted realistic heat fluxes and wind with data assimilation of observed wind and sea surface temperature (SST) (Chen et al., 2005). The major modification was the inclusion of the COARE 2.6 bulk algorithm (Fairall et al., 1996) into MM5 to improve the accuracy of heat flux calculation, with careful validations via the long-term field measurement made over Georegs Bank (Chen et al., 2005). Using a 10 km horizontal resolution, hindcast assimilations with all available coastal C-MAN and meteorological buoy data and the satellite-derived sea surface temperature (SST) were conducted to construct a high-resolution wind and heat flux database over GOM and GB from 1978 to the present (Hu, 2008). The wind stress ellipses based on monthly

wind means and variations in the last twenty years showed that the wind field was characterized by strong temporal variations in both speed and direction. In spring, fall and winter the wind velocity varied considerably over time scales of hours to 3-7 days, due to frequent passages of atmospheric fronts and storms. It is clear that monthly mean wind velocities can not adequately represent the meteorological conditions on GB, particularly for spring and fall seasons during which no persistent prevailing wind pattern exists (Hu, 2008).

The UMASSD-WHOI research team has applied the unstructured grid Finite-Volume Coastal Ocean Model (FVCOM) to the GOM/GB region (hereafter referred to as GOM-FVCOM). They simulated the 3D flow field and water stratification in the GOM/GB region from 1995 to the present with realistic heat flux and wind forcing predicted by MM5. Both water currents and stratification varied over hourly to daily time scales as a result of nonlinear interaction of tidal, wind, and buoyancy-induced motions. Sub-tidal currents, defined as a 40-hour low-pass filtered velocity, were also dominated by large temporal and spatial variations. In spring and fall, frequent passages of cold-air fronts and storms led to large variations of water currents and vertical mixing in space and time, which directly affects the water movement over GB. These spatial and temporal current variations should be taken into account when the transport pathways for species of short pelagic life stages are estimated. The pelagic phase of sea scallop larvae is on a time scale of one month.

There is evidence that the hydrodynamic flow fields used in previous larval recruitment studies do not represent the physical environment on GB well. However, how this influences the trajectories of individual larvae and ultimately the results of dispersal

and retention experiments is unknown. Previous work has provided us valuable insight into the impact of hydrodynamic process on larval dispersal and settlement under specified physical forcing. The question raised here is: what level of uncertainty do those models produce when applied to larval tracking experiments in the study of fish and invertebrate recruitment dynamics on GB? In this paper, we address this question by conducting a series of sensitivity experiments to examine how large variations occur in Lagrangian individual larval tracking under different simplified physical conditions. The experiments were made using GOM-FVCOM, with the understanding that the findings from this model can be applicable to other models under the same physical setups.

NUMERICAL MODEL AND EXPERIMENT DESIGN

We focused the numerical experiments on the tracking of neutrally buoyant particles using the 3D Lagrangian method implemented in FVCOM (Chen et al., 2006a). This method determines the particle position by solving a nonlinear system of ordinary differential equations given as:

$$\frac{dx}{dt} = \vec{v}(\vec{x}(t), t) \quad (1)$$

where \vec{x} is the particle position at time t , $d\vec{x}/dt$ is the rate of change of the particle position in time and $\vec{v}(\vec{x}, t)$ is the 3D velocity field. Eq. 1 is discretized and integrated using an explicit fourth-order Runge-Kutta (ERK) method.

The 3D flow field was provided by GOM-FVCOM. FVCOM is a prognostic, unstructured-grid, free-surface, 3D primitive-equation coastal ocean circulation model originally developed by Chen et al. (2003b) and continually improved by a team effort (Chen et al., 2006a,b; Cowles, 2007). The governing equations of FVCOM are discretized in geographic space using an unstructured triangular grid in the horizontal and a terrain-following coordinate transformation in the vertical. The geometric flexibility in the grid makes this model capable of resolving complex irregular coastlines and steep bottom topography, while the finite-volume flux algorithm guarantees mass conservation for each control volume. FVCOM has been validated using idealized benchmark test problems (Chen et al., 2007; Huang et al., 2008) as well as realistic applications in many coastal regions (see: <http://fvcom.smast.umassd.edu>).

GOM-FVCOM was originally configured using a computational domain that covered the entire GOM/GB region bounded by an open boundary from New Jersey to the Nova

Scotia Shelf (Chen et al., 2008a). With increases in computer power, this model has evolved through several different generations with increasing mesh resolution on GB, coastal regions and the shelf break. A detailed description of the GOM-FVCOM domains is provided at the FVCOM development team website: http://fvcom.smast.umassd.edu/research_projects/GB/index.html. The numerical experiments conducted in this paper used the first generation GOM-FVCOM, which has a horizontal resolution of ~0.5-2.0 km and a vertical resolution of ~1.3-4 m (31 σ -levels) on GB (Cowles et al., 2008).

Four experiments were conducted to evaluate the sensitivity of larval trajectories to different physical setups (Table 1). Exp. 1 refers to a model setup in which the larvae were tracked under the full 3D flow field of GOM-FVCOM driven by the MM5 assimilated wind stress and heat fluxes, observed river discharge from the primary rivers of the Gulf of Maine, tidal forcing constructed from the five principal constituents of M_2 , S_2 , N_2 , K_1 and O_1 , and an upstream open boundary influx on the Nova Scotia shelf (see Cowles et al., 2008 for a more detailed description of the model setup). Hereafter we refer to Exp. 1 as the “comprehensive” case, with emphasis on the use of spatial-resolved high-frequency forcing. Exp. 2 refers to the case in which the setup was identical to Exp. 1 except that only the M_2 constituent was used for the open boundary tidal forcing. A comparison between Exp. 1 and Exp. 2 provides us a quantitative estimation of the relative contribution of the linear superposition and nonlinear interaction of major semidiurnal and diurnal tidal constituents to larval trajectories. Exp. 3 was a “diagnostic experiment” in which the forcing condition was the same as in Exp. 1 but the density field remained unchanged during the integration. This constant density field was

constructed using temperature and salinity from bi-monthly climatologically-averaged fields in September and October, similar to previous larval transport experiments made on GB (Tremblay et al., 1994). Exp. 4 was identical to Exp 1. except that a bi-monthly (September-October) climatologically-averaged constant surface forcing was used to drive the model. The wind stress was specified using a magnitude of 0.01 N m^{-2} and a direction of 39° from north and the net heat flux was specified by a constant value of $158 \text{ W m}^{-2} \text{ s}^{-1}$. To distinguish from Exp. 3, we refer to Exp. 4 as the “uniform forcing” case. A comparison of Exp. 3 and Exp. 4 with Exp. 2 allows us to quantitatively examine the impact of the spatial and temporal variation of water stratification, wind forcing and surface heat flux on larval trajectories and thus provides an objective assessment on the uncertainty of the previous modeling studies.

Individual neutrally-buoyant particles released in different regions and at different depths were tracked in each experiment to analyze their trajectory deviation caused by simplified physical assumptions and forcing. To examine the level of the impact of simplification of the physical conditions on the dispersal and settlement of scallop larvae on GB in fall, we repeated Exps 1-4 by tracking the trajectories of scallop larvae spawned in the fishery closed areas over the southern and northern flanks of GB and in the Great South Channel (GSC) (Fig. 1). The closed areas were established in 1994 and the scallop spawning stocks in these areas have since increased 25-fold (Murawski et al., 2000; Stokesbury et al., 2004; Hart and Rago, 2006). In the scallop larval tracking experiments, the larvae were tracked using a Lagrangian Individual-Based population dynamics Model (IBM).

The IBM used in this study was described in detail in Tian et al. (2009). It consists of 4 pelagic phases (egg, trochophore, veliger and pediveliger) and 3 benthic phases (juvenile, young adult and adult). In this model, individual development is based on age: eggs: < 2 days; trochophores: 2-5 days; veligers: 5-35 days; pediveligers: > 35 days; juveniles: < 2 years; young adults: 2-4 years; adults: > 4 years (Stewart and Arnold 1994; Tremblay et al., 1994). The pelagic life stages are essentially differentiated by their behavioral vertical migration and the benthic components are described by their reproductive capability. All the pelagic life stages are subject to current drifting, random walks and behavioral vertical migration. Eggs are spawned near the bottom and are subject to passive current drifting. After 2 days, eggs hatch into trochophores, which migrate upward to the upper water column with a migration speed of 0.3 mm s^{-1} (Tremblay et al., 1994). At day 5, trochophores develop into veligers, which are essentially subject to passive drifting in the upper water column (a minimum migration speed of 0.1 mm s^{-1} was applied to prevent them from being dispersed to the bottom by random walks). At the age of 35 days, veligers develop into pediveligers, which actively descend to the bottom at a speed of -1.7 mm s^{-1} and search for suitable substrate for settlement (Tremblay et al., 1994).

To avoid unrealistic computational requirements deriving from tracking each spawned egg, we employed the technique of Lagrangian ensemble particles with each particle as an ensemble of individuals at the time of release. The number of larvae in each ensemble particle is determined in two phases: the spawning period before the release and larval development after the release. During the spawning period before the release, the number of eggs in each ensemble particle is determined by the spawning activity, which was

assumed to have a normal distribution in time. During the larval development following the release, the number of larvae in each ensemble particle is subject to an instantaneous mortality of 0.25 day^{-1} (McGarvey et al., 1992).

In 2003, a comprehensive video survey of scallop abundance was conducted in the GB region (Stokesbury et al., 2004) and we used this data set to determine the spawning stock. We assumed an average of 50 million eggs per adult scallop during each spawning season (Langton et al., 1987). On GB, fall spawning generally occurs in late September or early October (Shumway et al., 1988; McGarvey et al., 1992; DiBacco et al., 1995). We assumed that the maximum spawning was on the 20th of September with a standard deviation of one week. The model was run over 3 months from Sep. 1 to Nov. 30 in each experiment using the 2003 forcing. Scallop spawning was simulated at each time step, but spawned eggs were first accumulated in an ensemble particle in each simulation cell. When the total number of eggs reached a pre-defined number ($>10^{12}$ individuals), that ensemble particle was released and a new ensemble particle started to form in the same simulation cell. Multiple ensemble particles can be thus formed in a single simulation cell according to the spawning stock density. For the experiment with the two closed areas, 1480 ensemble particles containing 69.6×10^{15} eggs were released during the simulation. The time step used for spawning and particle tracking was 120 seconds. This time step is sufficient to resolve the temporal variation in semidiurnal tidal currents over GB (Chen and Beardsley, 1998; Chen et al., 2003b). A vertical random walk (Visser, 1997) was included to simulate the influence of turbulent mixing on particle distributions. To avoid the unrealistic aggregation of larvae due to the numerical algorithm, the random walk was integrated over a shorter time step of 6 seconds (Chen and Beardsley, 1998). The vertical

eddy diffusivity was kept identical within one tracking time step while particle positions were updated at each random-walk time step. These numerical schemes were found capable of resolving particle tracking problems on GB and implemented in the FVCOM simulation system (Chen and Beardsley, 1998; Chen et al., 2003b).

PARTICLE TRACKING EXPERIMENT RESULTS

Individual particle tracking

Treating larvae as neutrally-buoyant passive particles within the 3D flow field, we compared the trajectories of individual particles released in the surface layer at four selected locations in the Great South Channel (GSC) and on the northern and southern flanks of GB where scallop aggregations were observed during a field video survey (Stokesbury et al., 2004). The particle trajectories differed when forced with different model setups (Fig. 2). For a particle released in the GSC (Fig. 2a), for example, Exp. 1 predicted that the particle followed local isobaths and drifted eastward along the northern edge of GB, while Exps 2-4 all showed that it moved southward along the 60 m isobath and entered Nantucket Shoals. For a particle released at the northern flank of GB (Fig. 2b), Exp. 1 and Exp. 3 predicted that the particle drifted along the 60 m isobath around the top of GB, but Exp. 2 and Exp. 4 showed that it moved from GB to the New England Shelf (NES). For a particle released in the eastern part of the southern flank (Fig. 2c), Exp. 1 predicted that the particle moved around the top of GB following the 60 m isobath, but Exps 2-4 showed that it drifted from GB to Nantucket Shoals; similar differences were also found for a particle released in the western part of the southern flank of GB (Fig. 2d).

The disparity of particle trajectories under different physical settings also occurred near the sea floor. For a particle released in the GSC (Fig. 3a), Exp. 1 showed that the particle drifted eastward along the 60 m isobath, while Exps 2-4 all predicted that it moved southward and entered Nantucket Shoals. Although particles released at the northeastern flank of GB moved clockwise around the bank in all the four experiments,

their speeds and trajectories were considerably different (Fig. 3b). For a particle released within the tidal mixing front at the 60 m isobath on the southern flank (Fig. 3c), Exp. 1 predicted that the particle essentially moved along the tidal mixing front with limited cross-frontal movement at the beginning, while Exps 2-4 showed that it crossed the frontal zone and entered the central mixed area. Similarly, the particle released at the 100 m isobath of the southern flank of GB moved slightly northward in Exp. 1, but southwestward in other experiments, particularly in Exp. 3 where the particle drifted over a distance four times as long as that observed in other experiments, due to a bias in the density gradient with fixed temperature and salinity fields (Fig. 3d).

Our experiments clearly demonstrate that particle trajectories are quite sensitive to physical settings in the hydrodynamic model. Several points are evident in our experiments. First, GB is a strongly nonlinear system in which temporal and spatial variation of tidal currents should be taken into account when tracking particles. Simplifying the Lagrangian velocity as a sum of Eulerian and first-order approximate Stokes drift velocities is invalid in this region, and the settlement patterns of larvae thusly predicted should be interpreted with caution. Second, the wind field varied considerably in time and space. Monthly-averaged surface forcing does not accurately represent the true physical conditions in the region. The model-predicted distribution and on-bank or off-bank transports of larvae under the “climatologic” forcing can be used for process-oriented studies but the results should not be over-stated. Third, although the M_2 tide is dominant over GB, the other major semi-diurnal and diurnal tidal constituents contribute to the tidal variation, and can have a direct impact on particle trajectories.

Dispersion of scallop larvae spawned in the closed areas

We compared the results of the spatial distribution of scallop larvae settlement after three months of simulation from September 1 to November 30, 2003 driven by the physical fields generated using the four experimental setups. For scallop larvae spawned in Closed Area I (CAI), the four experiments predicted different distributions of larvae settlement. Exp. 1 predicted abundant larvae settled over GB, particularly on the southern and southeastern flanks of GB (Fig. 4a). Exp. 2 also showed an abundant distribution of larvae over GB, but with more larvae drifted onto the top of GB (Fig. 4b) as compared with Exp. 1. Exp. 3 predicted more larvae dispersed to the central well-mixed region on GB and to the NES, but less settlement on the southern flank of GB and in the GSC (Fig. 4c). Exp. 4 resulted in more larvae dispersed onto the top of GB and to the NES than Exp. 1 (Fig. 4d). Field observations suggest that the depth range of sea scallop habitat over GB is 18-110 m (Hart and Chute, 2004). We defined the retention rate as the percentage of larvae settled in this defined range over GB and in the GSC to the total number of spawned individuals. Exp. 1 predicted the highest retention rate of the larvae spawned in CAI (97%), followed by Exp. 2 (92%) and Exp. 4 (86%) while Exp. 3 resulted in the lowest retention rate (64%). The effects of mortality were not included in the calculation of retention.

For the case with scallop larvae spawned in Closed Area II (CAII), Exp. 1 predicted abundant larvae settled in the GSC and on the southwestern flank of GB (Fig. 5a). Exp. 2 showed similar pattern of scallop larvae distribution to Exp. 1, but with more larvae drifted to the NES (Fig. 5b). Exps 3 and 4 generated quite different results from the previous two experiments. Most of the larvae in Exp. 3 drifted out of the domain with

limited settlement on the southwestern flank of GB and on the slope of the NES (Fig. 5c). Exp. 4 resulted in larvae patches at the southern end of GSC and at the shelf break along the 100 m isobath on the NES (Fig. 5d). The retention rate of the larvae spawned in CAII was 81% for Exp. 1, 85% for Exp. 2, but only 20% for Exp. 3 and 69% for Exp. 4.

A metric of abundance was computed by summing up the number of settled larvae in each ensemble particle in a given computational cell divided by the cell area. For larvae spawned in CAI, Exp. 1 predicted high larval abundance along the 60 m isobath on the southern flank of GB and in the GSC (Fig. 6a). Exps 2 and 4 predicted similar abundance distribution of settled larvae to Exp. 1, but with increased larval abundance in the central region of GB inside the 60 m isobath and on the NES (Figs 6b and d). Exp. 3 showed different larval distribution from the other three experiments. Most of the larvae retained in Exp. 3 settled on the top of GB instead of the southern flank (Fig. 6c). For the case with larvae spawned in CAII, Exp. 1 predicted abundant larvae settlement on the southern flank of GB and in the GSC (Fig. 7a). Although Exp. 2 predicted similar distribution patterns, the high-abundance patch was found further west, nearer to the NES (Fig. 7b). Only a small patch of high larval abundance was observed on the southwestern flank of GB in Exp. 3 (Fig. 7c). The high-abundance patch of settled larvae in Exp. 4 moved further westward to the NES with less larvae settled in the GSC and on the southern flank of GB as compared to Exps 1 and 2 (Fig. 7d).

DISCUSSION

Exp. 1 was the standard model run with realistic meteorological and tidal forcing. The difference between Exp. 2 and Exp. 1 was in the tidal forcing: five tidal constituents were in Exp. 1 while only the M_2 tide was considered in Exp. 2. Comparison of larval tracks driven by the model circulation fields of Exp. 1 and Exp. 2 demonstrates that the tidal variation due to the superposition of semi-diurnal and diurnal tides can directly affect the distribution and abundance of larval dispersal and settlement. The superposition of M_2 , N_2 and S_2 tides produces fortnightly and monthly variations of tidal currents and thus a modulation of the subtidal along-bank current. On the southern flank, Butman et al. (1983) found that the ratio of the fortnightly and monthly modulation of the along-bank current to the mean along-bank current on GB varies in space in a range of $\sim 0.1-0.5$ (dimensionless), which can produce an along-bank tidally rectified flow in an order of $\sim 1.6-2.0 \text{ cm s}^{-1}$. Although it is relatively small, it accounts for a large portion of the subtidal flow observed on the southern flank (the magnitude of the subtidal current on the southern flank is $\sim 3-10 \text{ cm s}^{-1}$). On the northern flank, the current is characterized by strong nonlinearity due to a large tidal excursion scale. The nonlinearity can be measured by the ratio of tidal excursion scale ($l_o = U/\omega$; U is the magnitude of tidal velocity and ω is the tidal frequency) to the topographic length scale (l_s : the cross-isobath scale of the bottom slope) (Chen et al., 2003a). At the release location of the first particle at the northwest end of the GSC, U for the M_2 tide is 100 cm s^{-1} , and thus $l_o \sim 7 \text{ km}$ ($3.6 \text{ (km h}^{-1}) \times 12.42 \text{ (h)} / (2\pi)$). At this point, the magnitudes of N_2 , S_2 , K_1 and O_1 tidal velocities are 29, 18, 15 and 4 cm s^{-1} , respectively, with a sum of 66 cm s^{-1} . For a given l_s , even considering only the M_2 tidal frequency, l_o could be 66% larger in the case with multiple

tides than in the case with the only M_2 tide. Similar results have been obtained at the release location of the second particle on the northeast flank of GB, where the M_2 tidal velocity is $\sim 105 \text{ cm s}^{-1}$ and the sum of the other tidal constituents account for 50% of the M_2 tidal velocity. Note here that the superposition of these five tidal constituents produces a nonlinear modulation effect, which is more complex than the estimation made only by the M_2 frequency. The intensity of nonlinearity is believed to be a key factor causing the differences in particle trajectories between the comprehensive and M_2 tide-forced simulations through changes in both the Stokes drifts and the Eulerian residual current.

Exp. 3 is an example of “diagnostic models” that were employed in several previous fish larvae models over GB (Lough et al., 1994; Tremblay et al., 1994). However, results from the present work indicate that the inclusion of realistic evolving density fields leads to different transport and spatial variability of settled individuals (Exp. 1) in comparison with that driven by bi-monthly averaged hydrography (Exp. 3). This result is consistent with the prognostic model runs under a bi-monthly averaged wind stress by Werner et al. (1996) and Page et al. (1999). Ignoring the temporal and spatial variation of water density underestimates the fluctuation of tidal mixing front, which seems to have a significant influence on larval transport over long-term simulations, since the life span of pelagic scallop larvae is about one month or longer.

Similarly, the wind over GB varied considerably in time, particularly in fall. This is evident in Fig. 8, which shows that the wind was dominated by frontal passages over time scales of 3-7 days in September-November, 2003. The monthly mean wind was very small compared with the variation. It is clear that the Lagrangian transport produced by

the constant wind stress significantly differs in both direction and speed from that produced by the realistic time-dependent wind stress (Figs 2 and 3). The flow fields driven by constant averaged wind stress (Exp. 4) smoothed the variations caused by wind stress fluctuation (Exp. 1). Comparison of the results from Exp. 4 and Exp. 1 clearly shows that the wind variation needs to be taken into account for larval transport models. This point was first stated by Lewis et al. (1994 and 2001) in a plankton transport study and then by Tian and Chen (2006) for inter-model comparison experiments on GB. The other important issue is the spatial variation of the wind stress, which was not resolved in previous larval transport studies due to the lack of the wind data coverage in the Gulf of Maine (Werner et al., 1996; Page et al. 1999). GB is a shallow region affected by the cold-air frontal passage and storms. Based on the criteria of wind stress > 0.2 Pa and duration longer than 12 hours defined by Butman et al. (2008), Chen et al. (2008b) identified 28 and 31 strong wind events (storms or air-frontal passages) in 2006 and 2007. During these events the wind stresses varied considerably in space. These spatial wind variations were well-represented in Exp. 1 but not in Exp. 3.

We note that the trajectory of the particle released near the bottom on the southern flank in Exp. 1 differs strongly from those predicted in other three simplified cases. It moved across the isobath towards the top of the bank, whereas it drifted southwestward along the local isobath in other experiments. Chen et al. (2008a) conducted a model-dye comparison experiment on GB and found that the meso-scale temporal variability of tidal mixing front directly affect the movement of particles near the bottom. We believe that the difference in the particle trajectory at that point is related to density gradient fluctuation, due to the modulation of multi-tidal interactions and also wind fluctuation,

which was well resolved in the comprehensive run (Exp. 1) but partially smoothed in other experiments.

Although our experiments were focused on GB and the adjacent coastal regions, the major finding from this work has a general application to the larval transport and dispersion studies in other coastal regions characterized with strong nonlinearity. Wolanski (1993) pointed out that the linear addition of wind-driven, tide-driven and Eulerian mean flows was invalid to simulate larval dispersal due to nonlinear interactions in reef systems in the Australian coastal regions. His points, however, have not received attentions over the years. The inter-method comparison presented here is aimed at understanding the importance of including multiple tidal constituents, spatial- and temporal-resolved stratification and winds in larval transport simulation. It is well known that larval recruitment plays a critical role in fishery population dynamics, and IBMs represent a typical approach to recruitment studies. However, since IBM are driven by the flow field predicted by hydrodynamics models, the reliability of IBM prediction relies on the reality and accuracy of the circulation models. Since there are no perfect hydrodynamic models, in order to avoid misleading or inaccurate estimation, sensitivity analyses of larval transport to the model-predicted flow fields should be conducted when the results are used for management purposes (Huret et al., 2006).

In summary, numerical experiments were conducted to examine the sensitivity of the sea scallop larvae dispersal and settlement on GB and in the GSC to the flow fields predicted by FVCOM under four different physical settings. Both passive tracer tracking and IBM experiments indicate that GB is a strong nonlinear dynamic system in which the circulation and larval dispersal is influenced by the nonlinear interaction and modulation

of semi-diurnal and diurnal tidal constituents and high-frequency variations in winds and stratification. Ignoring high-frequency variations in wind forcing and in the density field can lead to different distributions of larval settlement and abundance on GB. The previous larval transport model results, which were based on particle tracking approaches with either an assumption of weak nonlinearity or incomplete physical settings, should be interpreted with caution. The IBM scallop larval transport should be based on a more reliable physical model with comprehensive high-frequency forcing. Due to imperfection in hydrodynamics models, however, sensitivity studies of larval transport to physical settings need to be conducted to provide uncertainty estimates whenever an IBM is used to study fishery recruitment on GB.

ACKNOWLEDGEMENT

We thank the editor Dr. J. A. Runge and two anonymous reviewers for their constructive comments during the revision of this paper. This study was supported by the research programs of Scallop Fishery Assessment and New England Multispecies Survey at the School for Marine Science and Technology (SMAST), University of Massachusetts Dartmouth, through NOAA grants DOC/NOAA/NA04NMF4720332, DOC/NOAA/NA04NMF4720339, DOC/NOAA/NA05NMF4721131, DOC/NOAA/NA05NMF4721132, DOC/NOAA/NA06NMF4720096 and DOC/NOAA/NA06NMF4720097 and the US GLOBEC/Georges Bank Program through NOAA Grant NA160P2323 and NSF grants OCE0227679 and OCE-0234545. This paper is SMAST Contribution Series #09-0101, School for Marine Science and Technology, University of Massachusetts Dartmouth.

REFERENCES

- Beardsley, R.C., Butman, B., Geyer, W.R., and Smith, P. (1997) Physical oceanography of the Gulf of Maine: An update. In: *Proceedings of the Gulf of Maine Ecosystem Dynamics Scientific Symposium and Workshop Report 97-1*. Reg. Assoc. for Res. in the Gulf of Maine, Hanover, NH, pp. 39-52.
- Butman, B, Noble, M., Chapman, D.C., and Beardsley, R.C. (1983) An upper bound for the tidally rectified current on one location on the southern flank of Georges Bank. *J. Phys. Oceanogr.* 13: 1452-1460.
- Butman, B., Sherwood, C.R., and Dalyander, P.S. (2008) Northeast storms ranked by wind stress and wave-generated bottom stress observed in Massachusetts Bay, 1990-2006. *Cont. Shelf Res.* 28: 1231-1245.
- Chen, C.S. and Beardsley, R.C. (1998) Tidal mixing and cross-frontal particle exchange over a finite amplitude asymmetric bank: A model study with application of Georges Bank. *J. Mar. Res.* 56: 1163-1201.
- Chen, C.S., Xu, Q., Beardsley, R.C., and Franks, P.J.S. (2003a) Modeling Studies of the Cross-Frontal Water Exchange on Georges Bank: A 3D Lagrangian Experiment. *J. Geophys. Res.* 108: 3142, doi:10.1029/2000JC000390.
- Chen, C.S., Liu, L., and Beardsley, R.C. (2003b) An unstructured grid, finite-volume, three-dimensional, primitive equation ocean model: Application to coastal ocean and estuaries. *J. Atmos. Oceanic Technol.* 20: 159-186.
- Chen, C., Beardsley, R. C., Hu, S., Xu, Q., and Lin, H. (2005) Using MM5 to hindcast the ocean surface forcing fields over the Gulf of Maine and Georges Bank region. *J. Atmos. Oceanic Technol.* 22: 131-145.

- Chen, C., Beardsley, R.C., and Cowles, G. (2006a) An Unstructured Grid, Finite-volume Coastal Ocean Model FVCOM, User Manual. Technical Report SMAST/UMASSD-06-0602, University of Massachusetts Dartmouth, 313pp.
- Chen, C, Beardsley, R.C., and Cowles, G. (2006b) An unstructured grid, finite-volume coastal ocean model (FVCOM) system. *Oceanography* 19: 78-89.
- Chen, C., Huang, H., Beardsley, R.C., Liu, H., Xu, Q., and Cowles, G. (2007) A finite-volume numerical approach for coastal ocean circulation studies: comparisons with finite difference models. *J. Geophys. Res.* 112: C03018, doi:10.1029/2006JC003485.
- Chen, C., Xu, Q., Houghton, R., and Beardsley, R.C. (2008a) A model-dye comparison experiment in the tidal mixing front zone on the southern flank of Georges Bank. *J. Geophys. Res.* 113: C02005, doi; 10.1029/2007jc004106.
- Chen, C., Xu, Q., Xue, P., Tian, R.C., Cowles, G., Rothschild, B., and Beardsley, R.C. (2008b) The 2006-2007 Mass Bay eutrophication model simulation: hydrodynamics model components. *MWRA 2008 Modeling Service Rep.* 157pp.
- Cowles, G. (2007) Parallelization of the FVCOM coastal ocean model. *Int. J. High Perform. C.* 22: 177-193.
- Cowles, G.W., Lentz, S.J., Chen, C., Xu, Q., and Beardsley, R.C. (2008) Comparison of observed and model-computed low frequency circulation and hydrography on the New England Shelf. *J. Geophys. Res.* 103: C09015, doi:10.1029/2007JC004394.
- DiBacco, C., Robert, G., and Grant, J. (1995) Reproductive cycle of the sea scallop, *Placopecten magellanicus* (Gmelin, 1791), on northeastern Georges Bank. *J. Shellfish Res.* 14: 59-69.

- Fairall, C.W., Bradley, E.F., Rogers, D.P., Edson, J.B., and Young, G.S. (1996) Bulk parameterization of air–sea fluxes for Tropical Ocean Global Atmosphere Coupled Ocean–Atmosphere Response Experiment. *J. Geophys. Res.* 101: 3747–3764.
- Hart, D.R. and Chute, A.S. (2004) Sea Scallop, *Placopecten magellanicus*, Life history and habitat characteristics. *NOAA Technical Memorandum NMFS-NE 189*, 21pp.
- Hart, D.R. and Rago, P.J. (2006) Long-Term Dynamics of U.S. Atlantic sea scallop *Placopecten magellanicus* populations. *N. Am. J. Fish. Manag.* 26: 490-501
- Hu., S. (2008) Impacts of physical forcing on seasonal and interannual variability of nutrient in the Gulf of Maine and Georges Bank. PhD thesis, University of Massachusetts Dartmouth, 205pp.
- Huang, H., Chen, C., Cowles, G.W., Winant, C.D., Beardsley, R.C., Hedstrom, K., and Haidvogel, D.B. (2008) FVCOM validation experiments: Comparison with ROMS for three idealized barotropic test problems. *J. Geophys. Res.* 113: C07042, doi: 10.1029/2007JC004557.
- Huret, M, Runge, J.A., Chen, C., Cowles, G., Xu, Q., and Pringle, J.M. (2007) Dispersal modeling of early life stages: sensitivity analysis with application to Atlantic cod in the western Gulf of Maine. *Mar. Ecol. Prog. Ser.* 347: 261-274.
- Langton, R.W., Robinson, W.E., and Schick, D. (1987) Fecundity and reproductive effort of sea scallop *Placopecten magellanicus* from the Gulf of Maine. *Mar. Ecol. Prog. Ser.* 37: 19-25.
- Lewis, C.V.W., Davis, C.S., and Gawarkiewicz, G. (1994) Wind forced biological-physical interactions on an isolated offshore bank. *Deep-Sea Res. II* 41: 51-73.
- Lewis, C.V.W., Chen, C.S., and Davis, C.S. (2001) Effect of winter wind variability on

- plankton transport over Georges Bank. *Deep-Sea Res. II* 48: 137-158.
- Loder, J.W., Shen, Y., and Ridderinkhof, H. (1997) Characterization of three-dimensional Lagrangian circulation associated with tidal rectification over a submarine bank. *J. Phys. Oceanogr.* 27: 1729-1742.
- Lough, R.G., Smith, W.G., Werner, F.E., Loder, J.W., Page, F.H., Hannah, C.G., Naimie, C.E., Perry, R.I., Sinclair, M., and Lynch, D.R. (1994) Influence of wind-driven advection on interannual variability in cod egg and larval distributions on Georges Bank: 1982 vs 1985. *ICES Mar. Sci. Symp.* 198: 356-378.
- McGarvey, R., Serchuk, F.M., and McLaren, I.A. (1992) Statistics of reproduction and early life history survival of the Georges Bank sea scallop (*Placopecten magellanicus*) population. *J. Northwest Atl. Fish. Sci.* 13: 83-99.
- Miller, C.B., Lynch, D.R., Carlotti, F., Gentleman, W., and Lewis, C.V.W. (1998). Coupling of an individual-based population dynamic model of *Calanus finmarchicus* to a circulation model for the Georges Bank region. *Fish. Oceanogr.* 7: 219-234.
- Murawski, S.A., Brown, R., Lai, H.L., Rago, P.J., and Hendrickson, L. (2000) Large-scale closed areas as a fishery-management tool in temperate marine systems: The Georges Bank experience. *Bull. Mar. Sci.* 66: 775-798.
- Page, F.H., Sinclair, M., Naimie, C.E., Loder, J.W., Losier, R.J., Berrien, P.L., and Lough, R.G. (1999) Cod and haddock spawning on Georges Bank in relation to water residence times. *Fish. Oceanogr.* 8: 3212-3226.
- Shumway S.E., Barter, J., and Stahlnecker, J. (1988) Seasonal changes in oxygen consumption of the giant scallop, *Placopecten magellanicus* (Gmelin). *J. Shellfish Res.* 6: 89-95.

- Stewart, P.L. and Arnold, S.H. (1994) Environmental requirements of the sea scallop (*Placopecten magellanicus*) in eastern Canada and its response to human impacts. *Can. Tech. Rep. Fish. Aquat. Sci.* 2005: 1-36.
- Stokesbury, K., Harris, B.P., Marino II, M.C., and Nogueira, J.I. (2004) Estimation of sea scallop abundance using a video survey in off-shore U.S. waters. *J. Shellfish Res.* 23: 33-40.
- Tian, R.C. and Chen, C.S. (2006) Influence of model geometrical fitting and turbulence parameterization on phytoplankton simulation in the Gulf of Maine. *Deep-Sea Res. II* 53: 2808-2832.
- Tian, R.C., Chen, C.S., Stokesbury, K.D.E., Rothschild, B., Cowles, G., Xu, Q.C., Hu, S., Harris, B.P., and Marino II, M.C. (2009) Modeling exploration of the connectivity between sea scallop populations in the Middle Atlantic Bight and over Georges Bank. *Mar. Ecol. Prog. Ser.* in press.
- Tremblay, M.J., Loder, J.W., Werner, F.E., Naimie, C.E., Page, F.H., and Sinclair, M.M. (1994) Drift of sea scallop larvae *Placopecten magellanicus* on Georges Banks: a model study of the roles of mean advection, larval behavior and larval origin. *Deep-Sea Res. II* 41: 7-49.
- Visser, A.W. (1997) Using random walk models to simulate the vertical distribution of particles in a turbulent water column, *Mar. Ecol. Prog. Ser.* 158: 275-281.
- Werner, F.E., Page, F.H., Lynch, D.R., Loder, J.W., Lough, R.G., Perry, R.I., Greenberg, D.A., and Sinclair, M.M. (1993) Influence of mean 3-D advection and simple

behavior on the distribution of cod and haddock early life stages on Georges Bank.
Fish. Oceanogr. 2: 43-64.

Werner, F.E., Perry, R.I., Lough, R.G., and Naimie, C.E. (1996) Trophodynamic and advective influences on Georges Bank larval cod and haddock. *Deep-Sea Res. II* 43: 1793-1822.

Wolanski, E. (1993) Facts and numerical artifacts in modelling the dispersal of crown-of-thorns starfish larvae in the Great Barrier Reef. *Aust. J. Mar. Freshwater Res.* 4: 427-36.

FIGURE CAPTIONS

Figure 1. Summertime general subtidal circulation pattern over Georges Bank (reproduced from Beardsley et al., 1997) and the initial positions of the ensemble particles of sea scallop larvae spawned in the closed areas (based on Stokesbury et al. 2004). CAI: Closed Area I; CAII: Closed Area II; CC: Cape Cod; GB: Georges Bank; GSC: Great South Channel; NEP: Northeast Peak; NES: New England Shelf; NS: Nantucket Shoals. Black continuous lines are the contours of the 60, 100 and 200 m isobaths.

Figure 2. Particle trajectories in the surface layer from four initial locations (black dots) on Georges Bank predicted by the four simulation experiments. Exp. 1: Standard FVCOM comprehensive setup with 5 tidal constituents; Exp. 2: Only M_2 tide was considered at the open boundary; Exp. 3: Temperature and salinity were kept constant during the simulation; Exp. 4: Uniform, seasonally averaged surface wind forcing and heat flux were used (see Table 1 for details). Black continuous lines are the contours of the 60, 100 and 200 m isobaths. Shaded areas indicate mixed regions inside the 60 m isobath.

Figure 3. Particle trajectories in the bottom layer predicted by the four simulation experiments defined in Fig. 2 and Table 1. Black continuous lines are the contours of the 60, 100 and 200 m isobaths. Shaded areas indicate mixed regions inside the 60 m isobath.

Figure 4. Settlement of scallop larvae ensemble particles released from Closed Area I (CAI) predicted by the four simulation experiments defined in Fig. 2 and Table 1. Black continuous lines are the contours of the 60, 100 and 200 m isobaths.

Figure 5. Settlement of scallop larvae ensemble particles released from Closed Area II (CAII) predicted by the four simulation experiments defined in Fig. 2 and Table 1. Black continuous lines are the contours of the 60, 100 and 200 m isobaths.

Figure 6. Abundance distribution of settled scallop larvae spawned in Closed Area I (CAI) predicted by the four simulation experiments defined in Fig. 2 and Table 1. Black continuous lines are the contours of the 60, 100 and 200 m isobaths.

Figure 7. Abundance distribution of settled scallop larvae spawned in Closed Area II (CAII) predicted by the four simulation experiments defined in Fig. 2 and Table 1. Black continuous lines are the contours of the 60, 100 and 200 m isobaths.

Figure 8. Hourly wind pattern and monthly averages in September through November 2003 on top of Georges Bank with the variance-based wind ellipse. Note: Different scales for the ordinate axis were employed to accommodate the larger magnitude of wind stress in the fall.

Table 1. Experiment design.

Experiment	Forcing
Exp. 1	Five tidal constituents (M_2 , S_2 , N_2 , K_1 and O_1), temporally and spatially resolved wind, heat fluxes and stratification, river discharges, Nova Scotia Shelf inflow.
Exp. 2	Same as Exp. 1 but only M_2 tide.
Exp. 3	Same as Exp. 1 but constant density (temperature and salinity).
Exp. 4	Same as Exp. 1 but constant and uniform wind and heat fluxes.

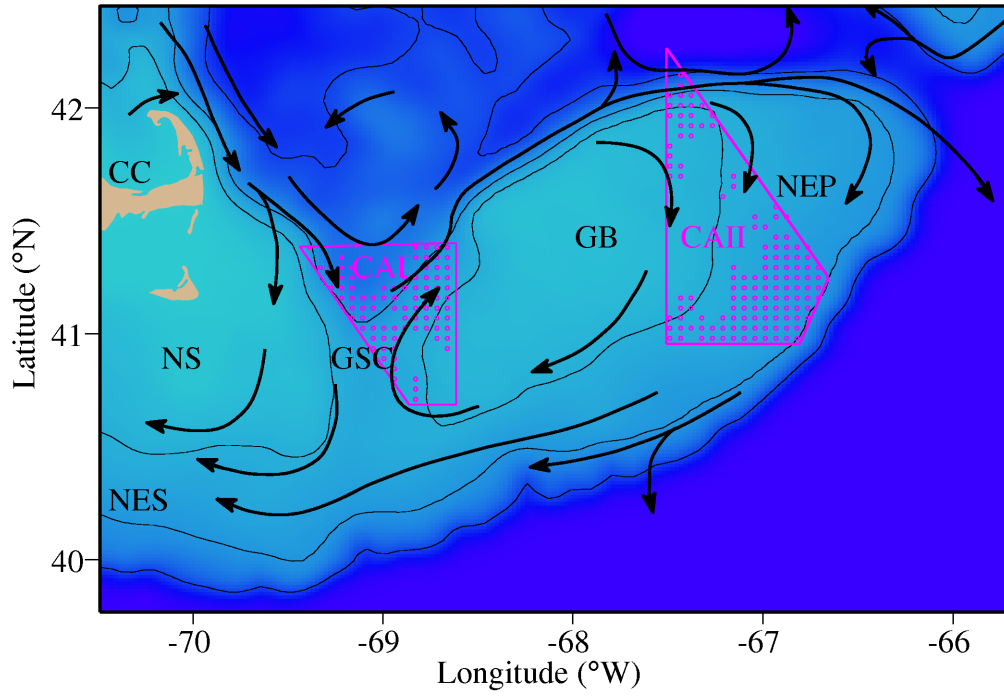


Fig. 1

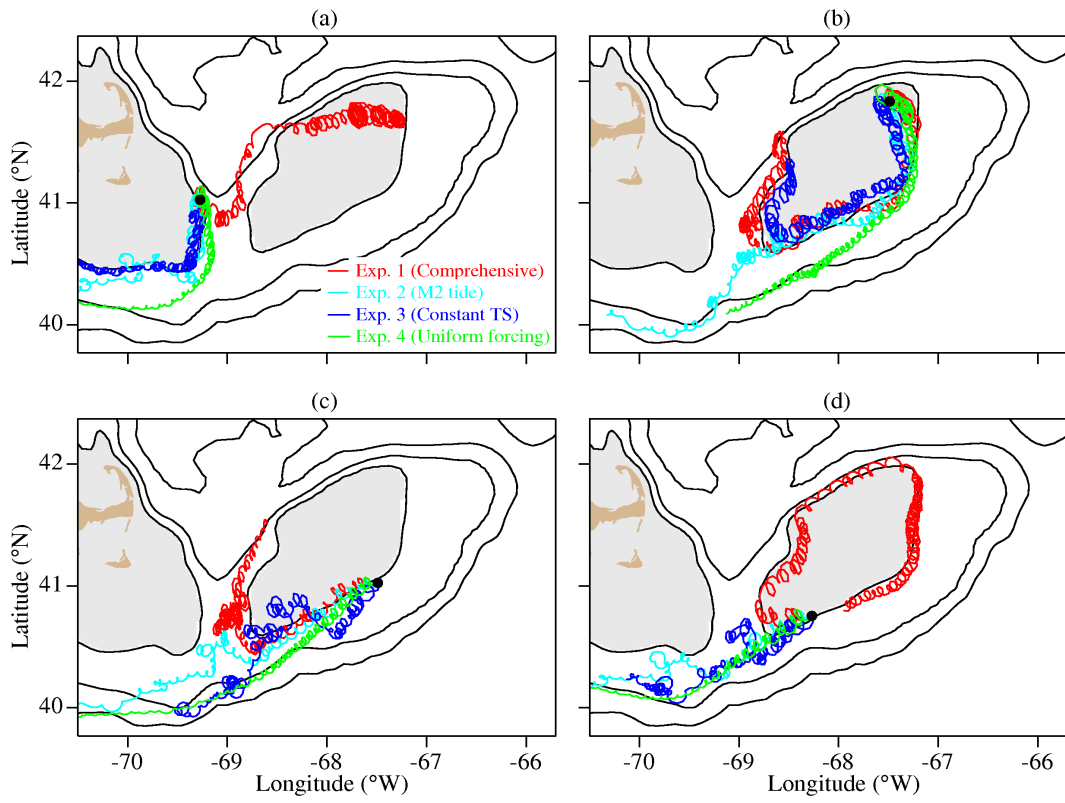


Fig. 2

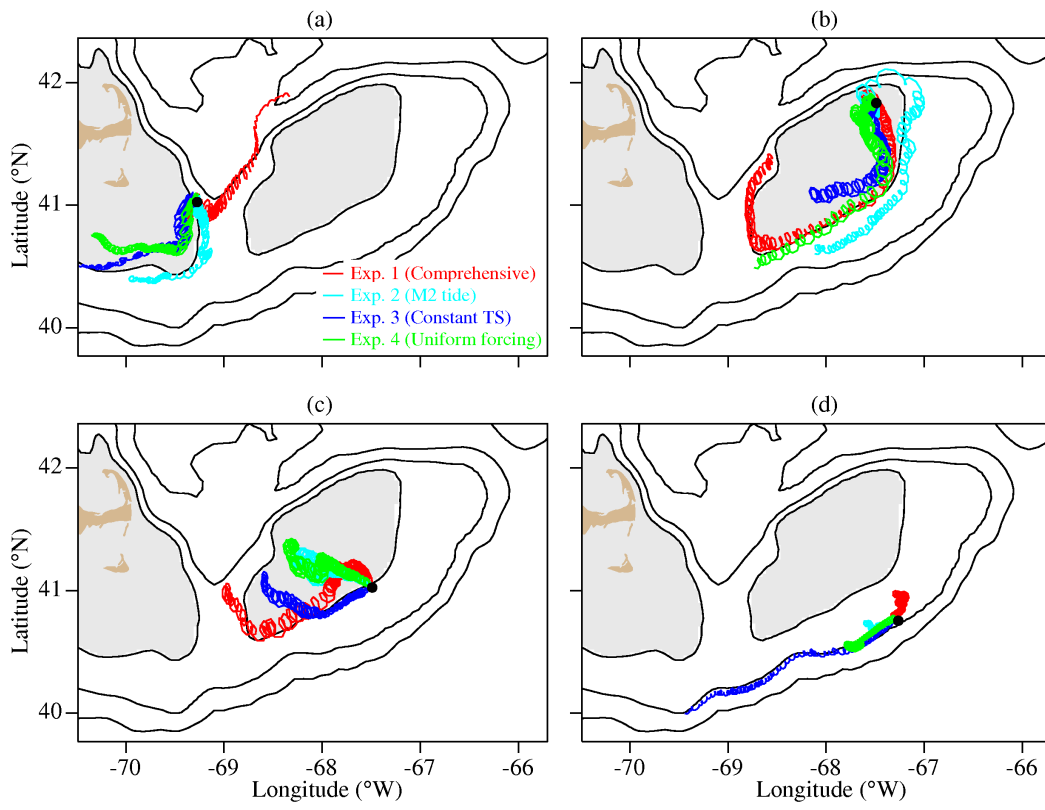


Fig. 3

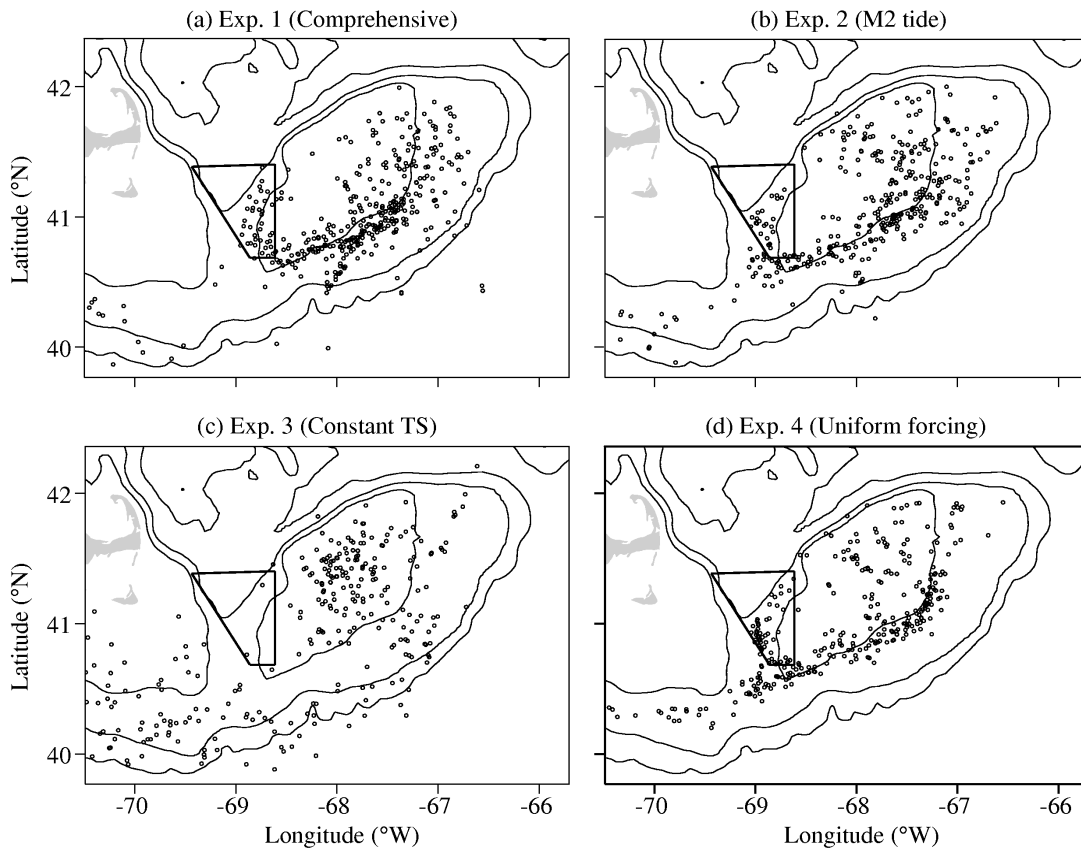


Fig. 4

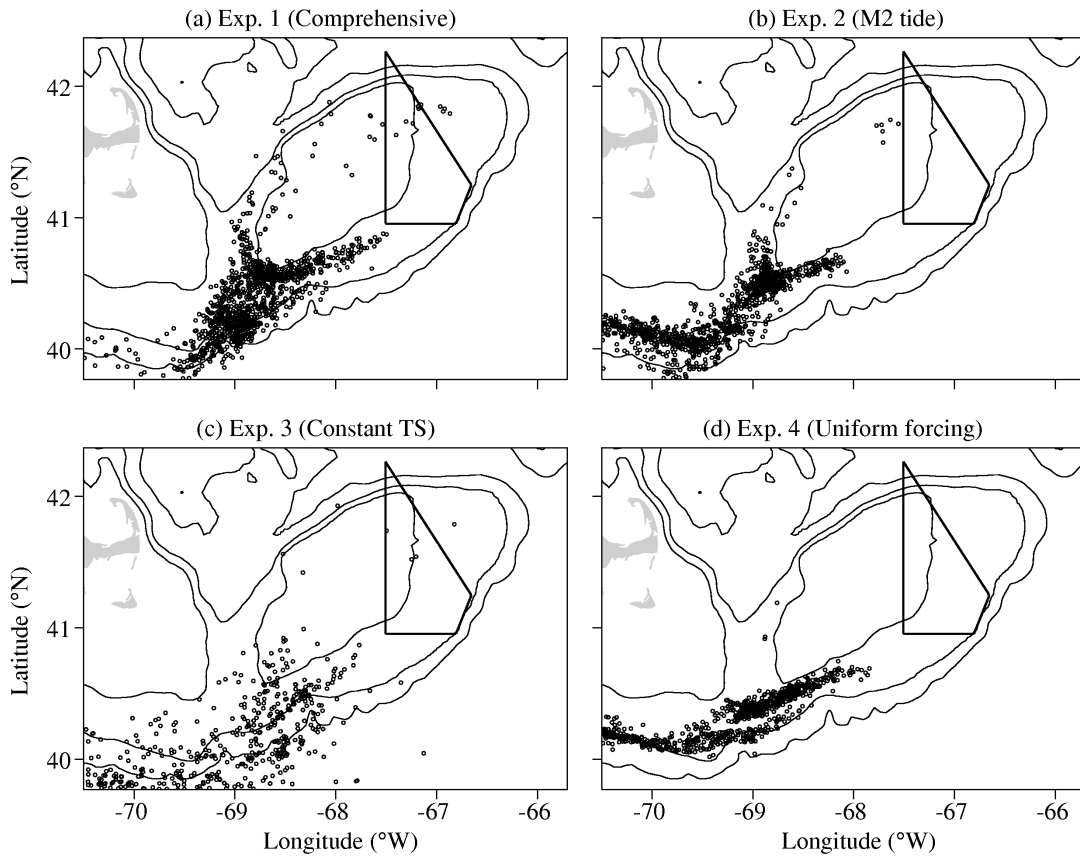


Fig 5

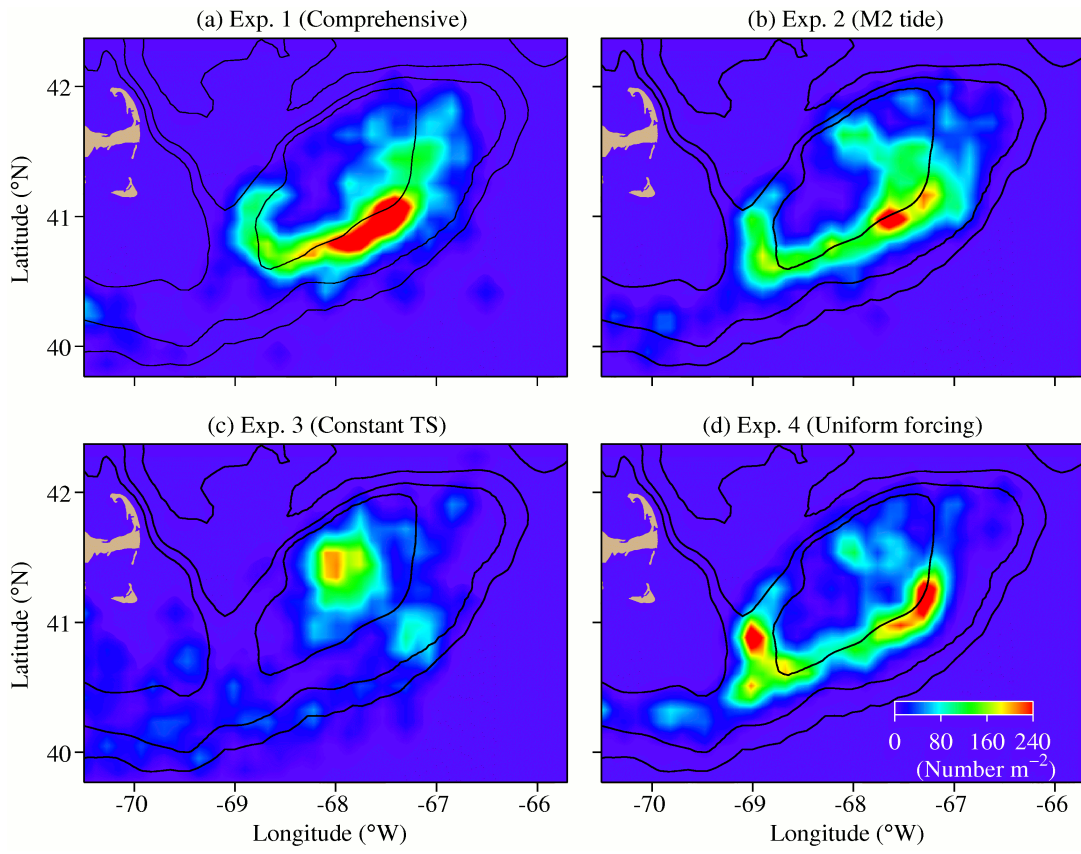


Fig. 6

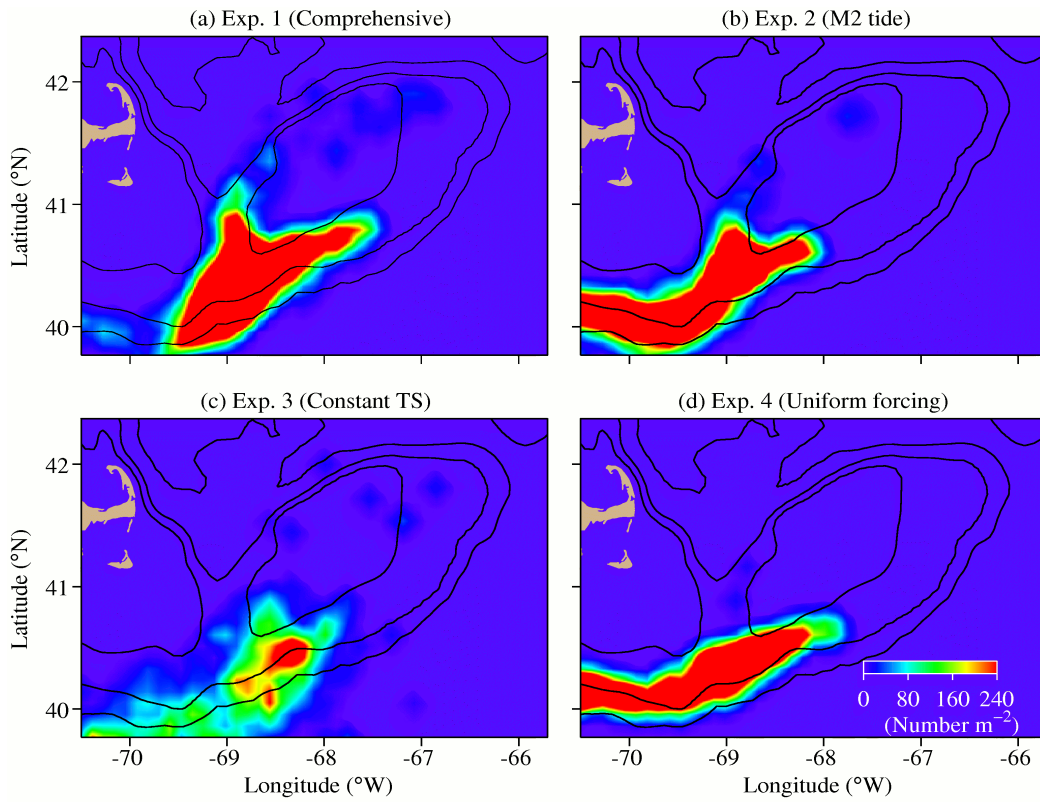


Fig. 7

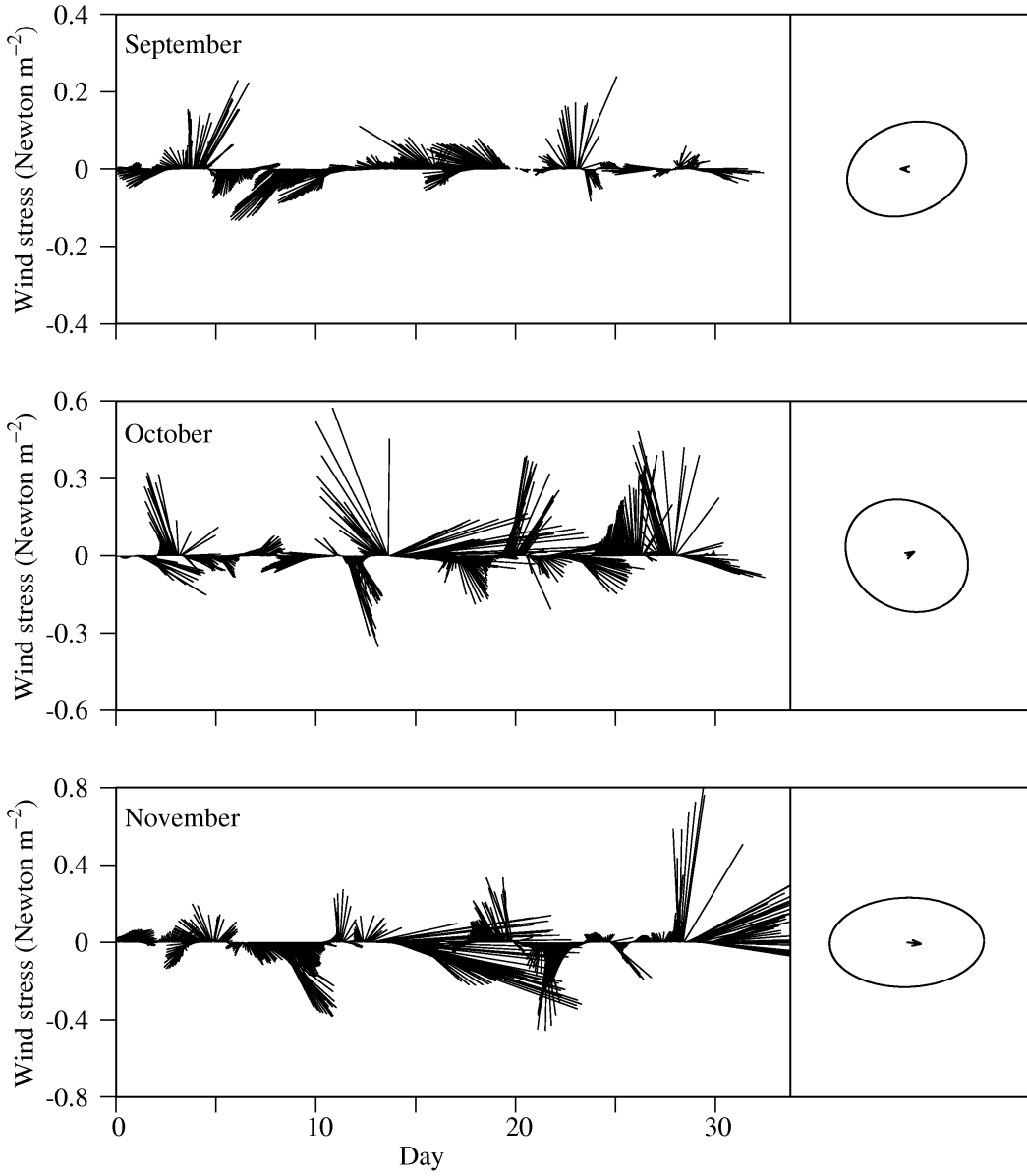


Fig. 8